analytical chemistry

pubs.acs.org/ac

Article

Discovery of a Phage Peptide Specifically Binding to the SARS-CoV-2 Spike S1 Protein for the Sensitive Phage-Based Enzyme-Linked Chemiluminescence Immunoassay of the SARS-CoV-2 Antigen

Junchong Liu,[†] Pengxin Ma,[†] Haipeng Yu, Mingyang Wang, Pengxue Yin, Shuang Pang, Yiming Jiao, Tao Dong, and Aihua Liu*

Cite This: *Anal. Chem.* 2022, 94, 11591−11599

Read Online

ACCESS | Metrics & More | Article Recommendations | Supporting Information

ABSTRACT: The COVID-19 pandemic has led to a global crisis with devastating effects on public healthcare and the economy. Sensitive detection of SARS-CoV-2 is the key to diagnose and control its spread. The spike (S) protein is an abundant viral transmembrane protein and a suitable target protein for the selective recognition of SARS-CoV-2. Here, we report that with bovine serum albumin prescreening, a specific phage peptide targeting SARS-CoV-2 S1 protein was biopanned with the pIII phage display library. The identified phage #2 expressing the peptide (amino acid sequence: NFWISPKLAFAL) shows high affinity to the target with a dissociation constant of 3.45 ± 0.58 nM. Furthermore, the identified peptide shows good specificity with a binding site at the N-terminal domain of the S1 subunit through a hydrogen bond network and hydrophobic interaction, supported by molecular docking. Then, a sandwiched phage-based enzyme-linked chemiluminescence immunoassay (ELCLIA) was established by using phage #2 as a bifunctional probe capable of SARS-CoV-2 S1 antigen recognition and signal amplification. After optimizing the conditions, the proposed phage ELCLIA exhibited good sensitivity, and as low as 78 pg/mL SARS-CoV-2 S1 could be detected. This method can be applied to detect as low as 60 transducing units (TU)/mL SARS-CoV-2 pseudovirus in 50% saliva. Therefore, specific phage peptides have good prospects as powerful biological recognition probes for immunoassay detection and biomedical applications.

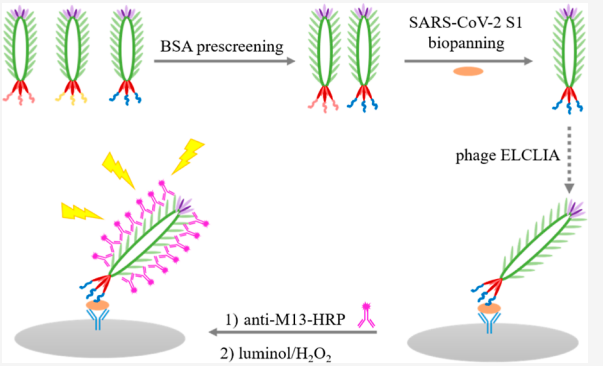

INTRODUCTION

The coronavirus disease 2019 (COVID-19) pandemic has led to a global crisis with devastating effects on public health and economy around the world. COVID-19 is caused by severe acute respiratory syndrome coronavirus 2 (SARS-CoV-2). Since December 2019, several variants of concern (VoCs) have emerged, such as B.1.1.7 (British variant; alpha), B.1.351 (South African variant; beta), P.1 (Brazilian variant; gamma), B.1.617.2 (Indian variant; delta), and B.1.1.529 (Omicron).[1] Some SARS-CoV-2 mutant variants have demonstrated reduced susceptibility to the vaccine or infection-elicited antibodies.[2] There are four main proteins encoded by the SARS-CoV-2 genome: spike (S) protein, nucleocapsid (N) protein, membrane (M) protein, and envelope (E) protein.[3,4] Among them, the S protein is a type I fusion protein and plays an important role in the process of virus infection and pathogenesis.[5] The S protein consists of two subunits: the S1 subunit is composed of the N-terminal domain (NTD) and receptor binding domain (RBD), which binds to cells expressing viral receptors, while the S2 subunit mediates fusion between the virus and the cell membrane.[6,7] S protein is an abundant viral transmembrane protein, and the amino acid sequence of this glycoprotein is different from other coronaviruses, so S protein is a suitable target protein for selective recognition of SARS-CoV-2.

The reverse transcription polymerase chain reaction (RT-PCR) is the most frequently used molecular assay due to its advantages of high throughput, high sensitivity, and specificity, but it has the problems of high cost and too complicated operation for unskilled laboratory technicians.[8,9] While serological tests are inexpensive and have a short analysis time, they are not suitable for diagnosing COVID-19 in the early stages of infection because antibodies are produced 10−14 days after infection.[10,11] Viral antigens can be used as specific markers of viral infection and significantly precede the patient's antibody response. Antigen testing provides an

Received: May 6, 2022
Accepted: July 29, 2022
Published: August 10, 2022

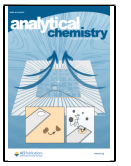

opportunity for early diagnosis and interruption of transmission through targeted isolation and grouping of most infected cases and their close contacts. Rapid antigen tests are easier to administer than molecular tests, provide clinical point-of-care results, and are less expensive than molecular tests, enabling self-testing.[12] Rapid antigen testing could reduce the prevalence of COVID-19 by an estimated 70% compared to unchecked growth.[13] With the surge in asymptomatic infections, the World Health Organization ensures that all countries have access to and use high-quality rapid antigen tests to effectively respond to a global pandemic [statement on the 10th meeting of the International Health Regulations (2005) Emergency Committee regarding the COVID-19 pandemic]. Previous studies have shown that asymptomatic and presymptomatic people infected with SARS-CoV-2 may have high viral loads, especially during sample testing during acute infection (within 5−7 days of symptoms appearing in the suspected population), so antigen testing can be an effective detection strategy, which can reduce the efficiency of virus transmission by finding the source of infection as early as possible.[14]

Sensitivity and selectivity are critical issues for the analytical method or sensor development, especially in diagnosing epidemic diseases including COVID-19.[15] Apparently, it is challenging to explore the highly specific molecular recognition element and sensitive signal amplification system, which play a significant role in developing robust analytical techniques.[16] The Ff phages (M13, f1, or fd) are filamentous viruses, composed of major capsid protein pVIII and minor capsid proteins pIII, pVI, pVII, and pIX, which are arrayed around the circular single-stranded DNA by electrostatic interaction. For example, 2700 copies of pVIII proteins are symmetrically exposed on the three-dimensional (3D) M13 phage (Scheme S1). On the other hand, phages are stable under harsh conditions including extreme pHs (pH 2−12), heating, nuclease,[17,18] and nonaqueous solvents.[19] Additionally, the specific phage monoclones could be amplified in scale-up by simple culture. Phage display technology is an in vitro method for the selection of specific fusion peptides displayed on the surface of phages.[20,21] Peptide phage libraries containing billions of variants are to interact with target molecules, and the most specifically bound peptides are enriched after 3−5 rounds of biopanning, and specific peptides can be selected by affinity from a large number of clones. Thus, considering the biocompatibility, multivalency, stability, and high structural homogeneity, specific peptide-displaying phages are ideal molecular recognition elements in biochemical analysis, biosensing, and bio-nanomedicine.[22−30]

In this work, we screen a phage monoclone expressing a NFWISPKLAFAL peptide from the pIII phage display library against the SARS-CoV-2 S1 antigen. The identified peptide exhibits high affinity and specificity for SARS-CoV-2 S1, which can be used as an antigen recognition probe. The pVIII proteins of the M13 phage are capable of providing multiple binding sites (∼2700 copies) for the anti-M13 antibody as a signal antibody. Thus, the highly ordered recombinant M13 phage is an amazing bifunctional probe with antigen recognition and signal amplification functions, by which enzyme-linked chemiluminescence immunoassay (ELCLIA) is established for SARS-CoV-2 S1. After optimizing the ELCLIA conditions, sensitive and selective detection of the SARS-CoV-2 S1 antigen is realized. Finally, the proposed method is applied to detect the SARS-CoV-2 pseudovirus in saliva with good sensitivity.

EXPERIMENTAL SECTION

Chemicals and Reagents. The Ph.D.-12 phage library with ∼1×10^{13} pfu/mL in titer, was purchased from the New England Biolabs (NEB, Beverly, MA, USA). The recombinant proteins of SARS-CoV-2 S1, SARS-CoV-2 RBD, SARS-CoV-2 NTD, SARS-CoV S1, SARS-CoV-2 NP, SARS-CoV NP, and SARS-CoV-2 (D614G) pseudoviruses were obtained from Novoprotein Co. (Shanghai, China). MERS-CoV S1 was obtained from ABclonal Technology Co. Ltd. (Wuhan, China). Horseradish peroxidase (HRP)-conjugated anti-M13 monoclonal antibody (anti-M13-HRP) and anti-SARS-CoV-2 S1 mAb were bought from Sino Biological (Beijing, China). 3,3′,5,5′-Tetramethylbenzidine (TMB) and luminol were purchased from TCI Co., Ltd (Shanghai, China). Bovine serum albumin (BSA) was purchased from Solarbio Life Sciences.

Apparatus. A high-speed CF16RXII refrigerated centrifuge (Hitachi, Japan) was used to centrifuge the phages. A Kylin−Bell microporous quick shaker (Haiyang, China) was used to incubate and wash the phage. The U-2910 spectrophotometer (Hitachi, Japan) and SPARK 10 M multifunction microplate reader (Tecan, Switzerland) were used to record the UV−vis spectra and measure absorbance. ELCLIA was carried out with an HTF-1 chemiluminescence reader (Qingdao, China).

Biopanning of Phages that Bind to SARS-CoV-2 S1 with Good Affinity and Specificity. *Biopanning of Phages Binding to SARS-CoV-2 S1 with Good Affinity.* In brief, 10 μg/mL SARS-CoV-2 S1 (150 μL) was added to the well of the microtiter plate and incubated overnight with gentle oscillation at 4 °C. After washing the well with TBST, 10 μg/mL BSA (150 μL) was added and let to stand at 4 °C for 1 h. After that, a 10 μL Ph.D.-12 phage library was added to the well and incubated with gentle oscillation at room temperature (RT) for 2 h. The well was washed 10 times with 0.1% TBST to remove any unbound phages. The bound phages were eluted by glycine-HCl buffer (0.2 M, pH 2.2, containing 1 mg/mL BSA, 0.1 mg/mL phenol red) with oscillation at RT for 20 min. The obtained eluant was neutralized with 15 μL of 1 M Tris-HCl buffer (1 M, pH 9.1). 100 μL of TBS was added to rinse the well with oscillation at RT for 10 min. The above solutions are mixed together. The BSA-negative selection was added to rounds 2, 3, and 4 biopanning. That is, the phage was incubated with BSA for 4 h before incubating the phage with SARS-CoV-2 S1. The phage titer was calculated, and the amplified product entered the next round of biopanning. Among them, the phage incubation time for rounds 2, 3, and 4 was shortened to 1.5, 1, and 1 h, respectively, and the concentration of Tween-20 in TBST also changed to 0.25, 0.25, and 0.5%, accordingly. The phage recovery rate (the ratio of output to input) was calculated between each round of biopanning.

After the 4 rounds of biopanning, 22 blue plaques were randomly selected and amplified with *E. coli* ER2738. The single-stranded circular DNA genome was extracted, purified, and then sent to Liuhe Centre of BGI Technology Co., Ltd (Qingdao, China) for sequencing. The amino acid sequences from the DNA sequences were analyzed. The phage monoclones were amplified.

1 μg/mL SARS-CoV-2 S1 (100 μL) was aliquoted into a 96-well microtiter plate and gently oscillated overnight at 4 °C.

https://doi.org/10.1021/acs.analchem.2c01988
Anal. Chem. 2022, 94, 11591−11599

BSA was used as a negative control. The wells were washed with 0.5% PBST, and then, 10 μg/mL BSA was added and left standing at 4 °C for 1 h. Then, the wells were washed three times with 0.5% PBST, and the selected phage monoclonal diluents (100 μL) were added and incubated with gentle oscillation at RT for 2 h. The wells were washed six times with 0.5% PBST. Anti-M13-HRP mAb (1:12,000, 100 μL) was added to the wells and gently oscillated at RT for 1.5 h. After washing six times with 0.5% PBST, the color was developed by adding a freshly prepared mixture of TMB and hydrogen peroxide. Finally, the reaction was terminated by 2 M H_2SO_4 (50 μL), and the optical density of each well at 452 nm (OD_{452nm}) was measured.

Testing the Specificity of the Selected Phage Monoclones. SARS-CoV-2 S1, SARS-CoV-2 RBD, SARS-CoV-2 NTD, SARS-CoV S1, MERS-CoV S1, SARS-CoV-2 NP, and SARS-CoV NP (each 2 μg/mL) were separately coated onto the wells with BSA as controls. Then, phage monoclonal was added to each well. After incubating with anti-M13-HRP (1:12,000), the mixture of TMB and hydrogen peroxide was added to develop the color, which was terminated with H_2SO_4, and the OD_{452nm} of each well was measured. The identified specific phage monoclones were applied for the following affinity testing.

Phage Monoclonal Affinity Assay. To determine the affinity of SARS-CoV-2 S1 to the obtained phage, SARS-CoV-2 S1 was immobilized in the wells and shaken overnight at 4 °C. Then, the wells were washed once with 0.5% PBST and blocked with 5 mg/mL BSA blocking buffer for more than 1 h at 4 °C. The wells were washed three times with 0.5% PBST. After the phage was serially diluted at a maximum concentration of 1.5×10^{13} pfu/mL, it was added to each well and incubated with shaking for 2 h at RT. Following a similar procedure to develop the color, the OD_{452nm} of each well was measured. The dissociation constant (K_d) was calculated by analyzing the binding curve of the selected phage using GraphPad Prism software.[31] The equation model used was $Y = B_{max} \times X/(K_d + X) + NS \times X + background$. B_{max} is the maximum specific binding in the same units as Y, K_d is the equilibrium dissociation constant in the same units as X, and it is the ligand concentration needed to achieve a half-maximum binding at equilibrium; NS is the slope of nonspecific binding in Y units divided by X units; the background is the amount of nonspecific binding with no added ligand.

Molecular Docking. To predict the possible interaction between the identified peptide and SARS-CoV-2 S1 protein, molecular docking was carried out. MOE2014 software was used to generate the equivalent 3D structure of peptides with known amino acid sequences. The 3D structure of the SARS-CoV-2 S1 protein was obtained from the RCSB PDB database (ID:7FG7).[32] Before molecular docking, MOE2014 was used to optimize the identified peptide of phage #2 and protein to remove protein ligands and residual water molecules. When the optimization was completed, the SiteFinder function of MOE2014 was used to find the most optimal docking site and obtain docking results.[33] The best interaction complex structure was obtained by docking results with the highest score.[33]

Establishment of the Phage-Based ELCLIA. *General Procedure.* Anti-SARS-CoV-2 S1 mAb was immobilized in a 96-well white microplate overnight at 4 °C. The wells were washed once with 0.5% PBST and blocked with a blocking solution (containing 5% glycine, 0.5% alginate, and 0.05% PBST) at RT for 2 h. After washing three times with 0.5% PBST, SARS-CoV-2 S1 was added and incubated with shaking for 1.5 h at RT. Subsequently, the wells were washed twice with 0.5% PBST and a phage diluent (0.5% casein and 5% glycerol dissolved in PBS) was added to incubate with shaking at RT for 1.5 h. Then, the wells were washed five times with 0.5% PBST, anti-M13-HRP was added, and the wells were incubated with shaking at RT for 1.5 h. After the wells were washed four times with 0.5% PBST, 100 μL of a mixture solution of 0.05 mM luminol and 0.5 mM hydrogen peroxide (1:1 v/v) was added, and the maximum relative light units (RLU_{max}) were measured per well using a chemiluminescence reader.

Optimization of Coating Buffers for the Antibody. In order to determine a better antibody coating buffer, different-pH coating buffers were tested to explore their effects on ELCLIA results. Anti-SARS-CoV-2 S1 mAb (0.5 μg/mL) was prepared with 50 mM PBS (pH 7.4), 50 mM TBS (pH 7.5), 50 mM TBS (pH 8.0), 50 mM Na_2CO_3/$NaHCO_3$ (CB, pH 8.6), and 50 mM Na_2CO_3/$NaHCO_3$ (CB, pH 9.6), respectively. Then, 100 μL was added to each well and incubated with shaking overnight at 4 °C. The subsequent steps were the same as the general procedure. Finally, the color development reaction was initiated by adding a luminol/hydrogen peroxide mixture to the arrays.

Optimization of the Anti-SARS-CoV-2 S1 MAb Dosage. To explore the effect of antibody coating concentration on antigen capturing ability, the anti-SARS-CoV-2 S1 mAb concentrations were set to 0.25, 0.5, 1, 2, and 4 μg/mL, of which 100 μL was separately added to the wells of the plate and incubated overnight at 4 °C with shaking. The subsequent steps were the same as the general procedure.

Optimization of SARS-CoV-2 S1 Antigen Incubation Time. The incubation times were set to 0.5, 1, 1.5, 2.5, and 3.5 h. Finally, the RLU_{max} values were measured and the best experimental conditions were selected for the later experiments.

Optimization of the Specific Phage Dosage. Based on the above optimal conditions, the specific phage #2 was serially diluted into 0.75×10^{10}, 1.5×10^{10}, 3×10^{10}, 6×10^{10}, and 12×10^{10} pfu/mL for use. The chemiluminescence intensities were recorded with SARS-CoV-2 S1-coated wells (positive value) and the wells without SARS-CoV-2 S1 (negative value). The ratios of positive to negative (P/N) were compared.

Optimization of Binding Time of the Phage Interacting with SARS-CoV-2 S1. Under the optimal conditions described above, the time when phage #2 interacted with SARS-CoV-2 S1 was optimized. The incubation time was set to 0.5, 1, 1.5, and 2 h. The subsequent steps were the same as above. The RLU_{max} values of each group were measured and the P/N ratios were compared.

Optimization of the Anti-M13-HRP Dilution Ratio. The dilution ratio of anti-M13-HRP mAb under the optimal conditions was set to 1:4000, 1:8000, 1:12,000, 1:20,000, and 1:40,000, and the optimal dilution ratio was selected according to the results.

Testing of the Detection Sensitivity of Phage ELCLIA to the SARS-CoV-2 S1 Antigen. Under optimal ELCLIA experimental conditions, wells were coated with anti-SARS-CoV-2 S1 mAb (1 μg/mL) and incubated overnight at 4 °C. After washing once with 0.5% PBST, a blocking solution was added and incubated for 2 h at RT. After washing, different

https://doi.org/10.1021/acs.analchem.2c01988
Anal. Chem. 2022, 94, 11591−11599

concentrations of SARS-CoV-2 S1 were added and incubated for 2.5 h, and washed twice. Then, phage #2 (6.0×10^{10} pfu/mL) was incubated for 1.5 h and washed five times, and 1:8000 anti-MI3-HRP mAb was added to incubate for 1.5 h at RT. After washing four times with 0.5% PBST, 100 μL of the luminol/hydrogen peroxide mixture solution was added and the RLU_{max} values were measured.

Detection of the SARS-CoV-2 Pseudovirus. The SARS-CoV-2 pseudovirus was first inactivated (65 °C for 30 min). Then, serial dilutions were performed with PBS buffer or 50% saliva of healthy individuals (1:1 v/v ratio of saliva to PBS buffer). ELCLIA experiments were performed with the optimal conditions above. Pseudovirus-related experiments were carried out inside a class II biological safety cabinet.

RESULTS AND DISCUSSION

Biopanning of Phages Specifically Binding to SARS-CoV-2 S1. *Biopanning of Phages Binding with SARS-CoV-2 S1 with Good Affinity.* The Ph.D.-12 phage library was used to perform biopanning of phages that specifically bind to SARS-CoV-2 S1 (Scheme S2). After four rounds of biopanning, the phage recovery rate increased round by round even if BSA negative screening was performed from the second round (Figure S1), indicating that the phages binding to SARS-CoV-2 S1 were effectively enriched. After four rounds of biopanning, the fourth round of eluate was plated and cultured, and 24 phage single clones were randomly selected for amplification and DNA extraction and sequencing. 8 sequences were successfully obtained from 24 phage monoclones (Table S1), which were selected to verify their binding ability to the target antigen. The phage monoclonal was regarded as positive, given that the absorbance of phage binding to the antigen was more than twice that of the negative control (BSA). As shown in Figure 1, the absorbance of phage #2 with the identified peptide PX2 (amino acid sequence, NFWISPKLAFAL) was 8.5 times that of the negative control, indicating that phage #2 was a positive monoclonal.

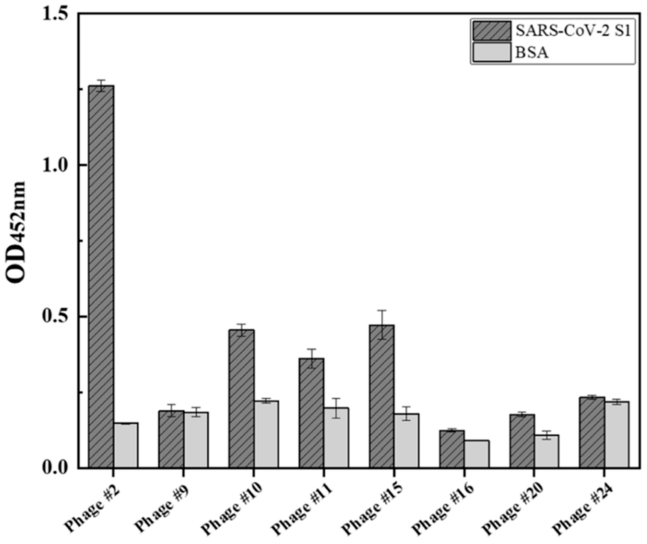

Figure 1. Phage ELISA method to determine the binding ability of eight selected phage monoclones to SARS-CoV-2 S1, with BSA as a negative control (n = 3).

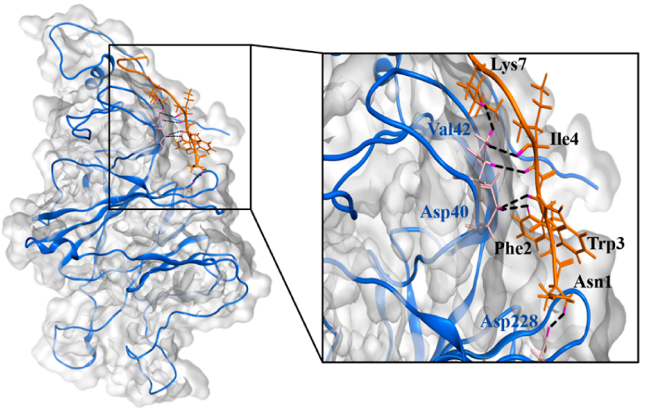

Figure 3. Molecular docking results. 3D interaction map of peptide PX2 and SARS-COV-2 S1. The Asn1, Phe2, Trp3, Ile4, and Lys7 of peptide PX2 are shown in yellowish brown. The Asp228, Asp40, and Val42 of the SARS-COV-2 S1 protein are shown in light pink. The dashed lines indicate hydrogen bonding.

Specificity and Affinity of Phage #2 to SARS-CoV-2 S1. Some key antigens (SARS-CoV-2 NTD, SARS-CoV-2 RBD, SARS-CoV S1, MERS-CoV S1, SARS-CoV-2 NP, and SARS-CoV NP) were selected for the specificity experiments (Figure 2A). Phage #2 did not bind to either SARS-CoV S1 or MERS-CoV S1, analogous antigens from coronaviruses, suggesting its

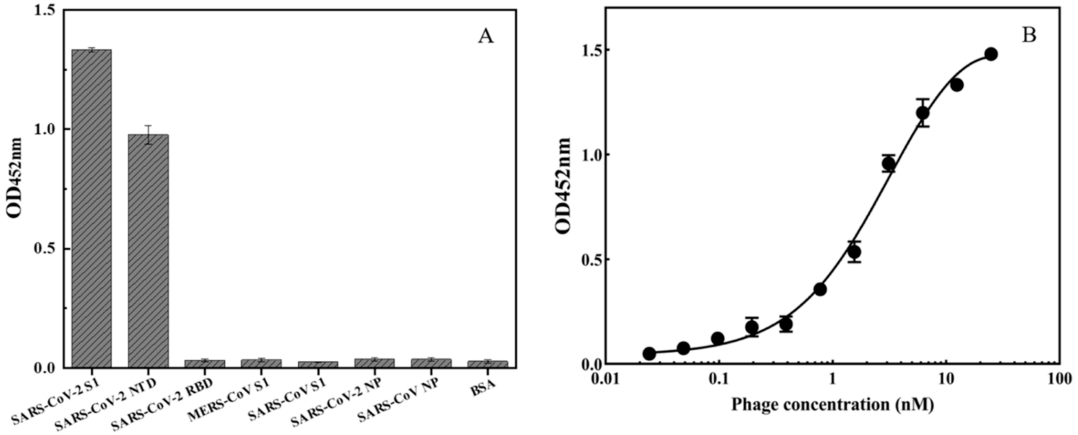

Figure 2. (A) Selectivity test of phage #2 binding to some key antigens (n = 3). (B) Binding curve of phage #2 interacting with SARS-CoV-2 S1 (n = 3).

https://doi.org/10.1021/acs.analchem.2c01988
Anal. Chem. 2022, 94, 11591−11599

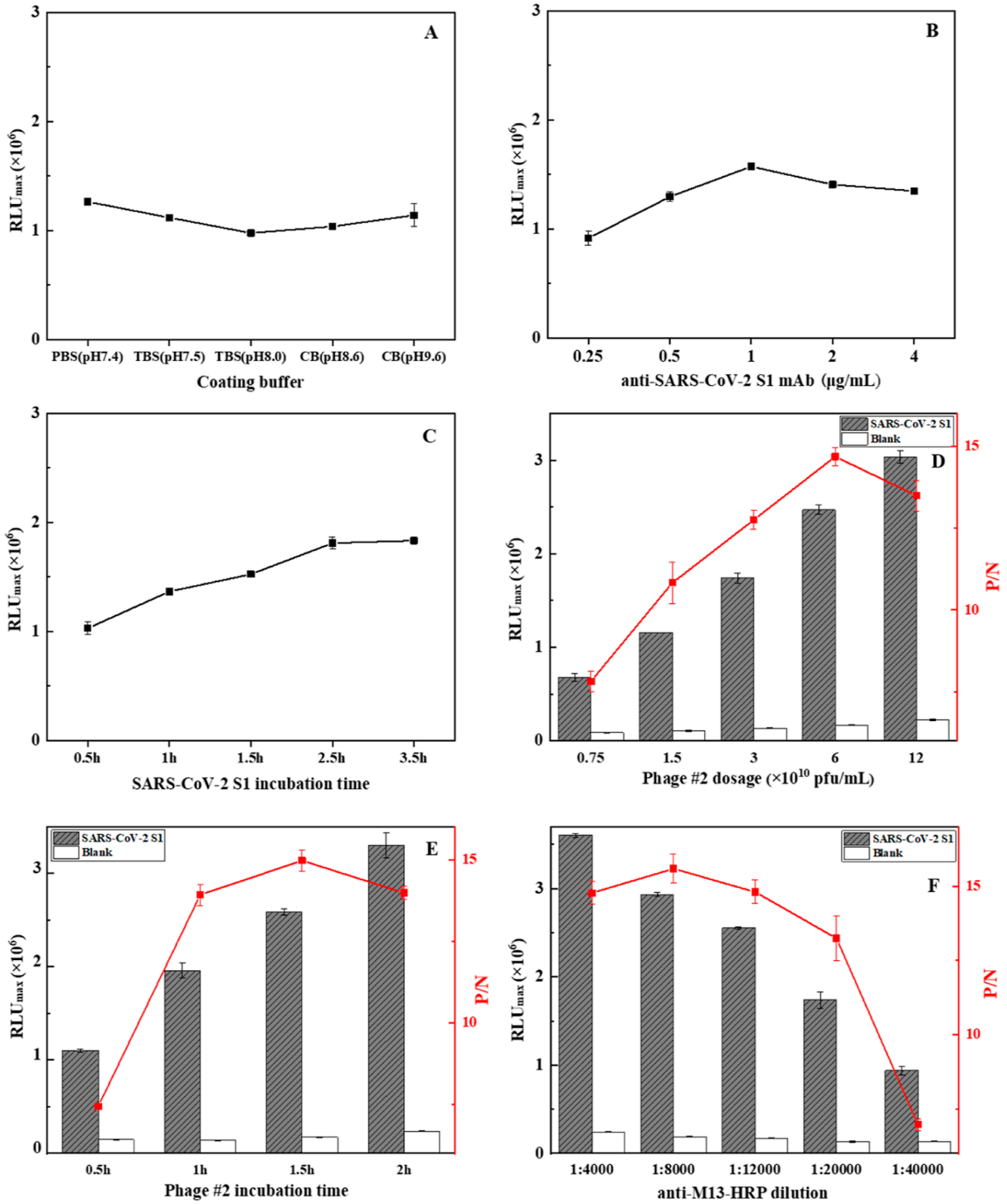

Figure 4. Optimization of ELCLIA conditions. Effects of (A) different coating solutions with 50 mM PBS (pH 7.4), 50 mM TBS (pH 7.5), 50 mM TBS (pH 8.0), 50 mM CB (pH 8.6), and 50 mM CB (pH 9.6), (B) anti-SARS-CoV-2 S1 mAb dosage, (C) antigen incubation time, (D) phage #2 dosage, (E) binding times of phage #2 to the antigen, and (F) anti-M13-HRP dilution (n = 3).

high selectivity to SARS-CoV-2 S1. Considering that the S1 subunit comprises an NTD and a RBD,[34] the specific sites were further investigated. Phage #2 showed good binding to SARS-CoV-2 NTD rather than SARS-CoV-2 RBD, inferring that the binding site of phage #2 to SARS-CoV-2 S1 might be at its NTD site. The binding curve of phage #2 interacting with SARS-CoV-2 S1 was obtained by ELISA (Figure 2B). After analysis of their binding curve with GraphPad Prism software, the K_d of the complex of peptide PX2 (NFWISPKLAFAL) of phage #2 and SARS-CoV-2 S1 was estimated as 3.45 ± 0.58 nM.

To Study Peptide Binding to SARS-CoV-2 S1 by Molecular Docking. The specific experiment shows that the selected peptide PX2 binds to the NTD of the SARS-CoV-2 S1 subunit. After taking into account the structure of NCBI S protein and SiteFinder operation, we finally determined the peptide binding region (Y38, K41... S45, V47, T167, D198, G199, E224, P230, G232, G232, N234, and P282). Twenty

https://doi.org/10.1021/acs.analchem.2c01988
Anal. Chem. 2022, 94, 11591−11599

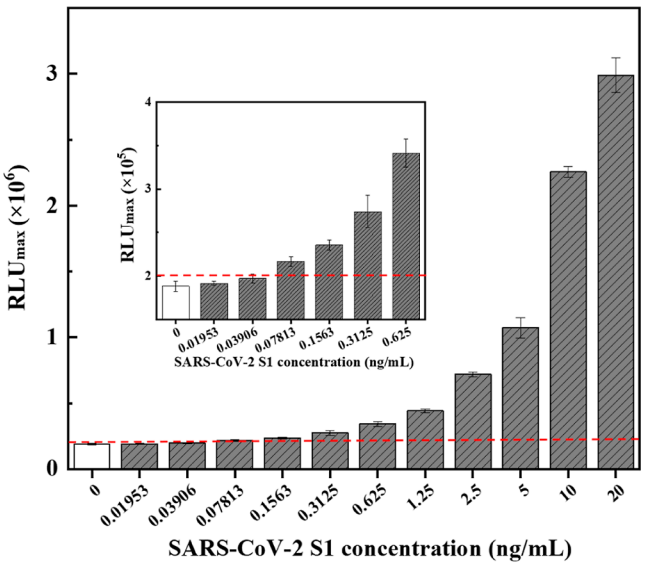

Figure 5. Detection of different concentrations of SARS-CoV-2 S1. The red dashed line is the LOD determined by the mean value of negative controls (0 ng/mL of SARS-CoV-2) plus 3 times the standard deviation (SD) (n = 3).

docking results (Table S2) were obtained. The docking between the peptide PX2 and SARS-CoV-2 S1 with the highest score (see the final score in the red frame, Table S2) suggests the lowest binding energy,[33] indicative of the formation of the best peptide−protein complex. It is obvious that a hydrogen bond network forms between the amino acid residues of peptide PX2 (Asn1, Phe2, Trp3, Ile4, and Lys7) and the amino acid residues of the SARS-CoV-2 S1 protein (Asp228, Asp40, and Val42) (Figure 3). Especially, a varying number of hydrogen bonds form between Asn1 and Asp228, Phe2 and Trp3 with Asp40, and Ile4 and Lys7 with Val42. The resultant hydrogen bond network should greatly stabilize the peptide−protein complex, which is also the possible reason for the identified peptide and SARS-CoV-2 S1 having good affinity.[35,36] Additionally, there exists hydrophobic interaction between peptide amino acid residues (Phe2 and Trp3) with those of S1(Asp40, Ile4, and Val42), by which the peptide PX2-SARS-CoV-2 S1 protein complex might maintain a stable conformation.[35,36]

Establishment and Optimization of the ELCLIA Based on Phage #2. Chemiluminescence analysis is an analytical method that combines chemiluminescence technology with the immunochemical reaction and has the advantages of good reproducibility, low cost, and rapid and accurate detection.[37] For the conventional sandwich ELCLIA, two antibodies are required, where the primary antibody is used to capture the antigen, which is then recognized by the secondary antibody, followed by signal amplification for detection. In this work, considering that phage #2 has a bifunction of specific affinity to antigen SARS-CoV-2 S1 and signal amplification after interaction with anti-M13-HRP, coupled with anti-SARS-CoV-2 S1 mAb as the capture, a phage-based sandwich ELCLIA was established for the detection of SARS-CoV-2 S1 (Scheme S3).

In order to improve the detection sensitivity, the main experimental parameters were optimized. The optimal coating buffer varies depending on the microplate type and immobilized proteins.[38] The effects of five different coating buffers were explored, and PBS (0.1 M, pH 7.4) was found better to immobilize anti-SARS-CoV-2 S1 mAb than other buffers (Figure 4A). The resultant RLU_{max} reached a peak when 1 μg/mL anti-SARS-CoV-2 S1 mAb was immobilized (Figure 4B). The RLU_{max} value increased gradually with increasing incubation time and reached a plateau at 2.5 h (Figure 4C). However, to our surprise, the RLU_{max} values remained unchanged with further incubation. Considering the simplicity of the reaction and the efficiency of the assay, incubation was performed for 2.5 h at RT. The dosage of phage #2 and the binding time are critical parameters. The RLU_{max} value was the highest when 12×10^{10} pfu/mL phage #2 was applied (Figure 4D). Interestingly, the P/N value of the applied phage at 6×10^{10} pfu/mL was higher than that of 12×10^{10} pfu/mL, which may be due to the higher background value with the higher amount of phage monoclones. As shown in Figure 4E, the P/N value peaked at a binding time of 1.5 h for phage #2 interacting with SARS-CoV-2 S1, which tended to decrease as the reaction time exceeded over 1.5 h. In our phage ELCLIA, phage #2 recognized the anti-SARS-CoV-2 S1 antigen captured by anti-SARS-CoV-2 S1 mAb, while anti-M13-HRP recognized the phage and acted as a signal amplifier.

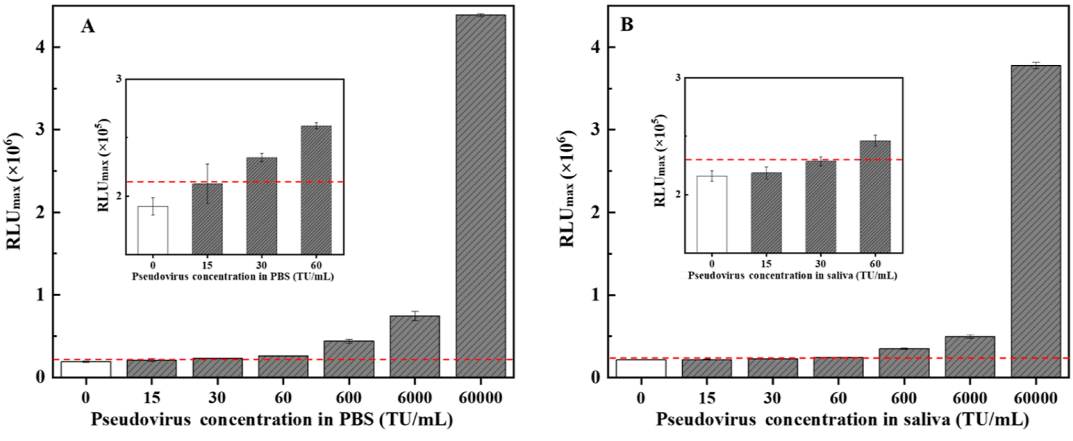

Figure 6. Phage ELCLIA detecting pseudo-SARS-CoV-2. (A) Detection of inactivated pseudoviruses in PBS. (B) Detection of inactivated pseudoviruses in 50% saliva. The red dashed line is the LOD determined by the mean value of negative controls (0 TU/mL of pseudo-SARS-CoV-2) plus 3 times the SD (n = 3).

https://doi.org/10.1021/acs.analchem.2c01988
Anal. Chem. 2022, 94, 11591−11599

The P/N value peaked at a 1:8000 dilution for anti-M13-HRP mAb (Figure 4F).

Sensitivity of the Phage-Based ELCLIA to Detect the SARS-CoV-2 S1 Antigen. To determine the sensitivity of the phage-based ELCLIA to detect SARS-CoV-2 S1, anti-SARS-CoV-2 S1 mAb was coated and a series of gradient concentrations of SARS-CoV-2 S1 were added. The RLU_{max} values were determined under the optimal ELCLIA conditions. The RLU_{max} values increased with standard concentrations of SARS-CoV-2 S1 (Figure 5). The limit of detection (LOD) was calculated as 0.078 ng/mL (~0.998 pM). The analytical performance of different methods for SARS-CoV-2 spike antigens is collected in Table S3. The LOD was reported for the surface plasmon resonance-based aptasensor (0.26 nM),[39] lateral flow immunoassay (LFIA) (>0.1 ng/mL),[40,41] the organic field effect transistor (OFET) (76.61 pg/mL),[42] nanomechanical sensor-based platform (1 ng/mL),[43] electrochemical immunosensor (19 ng/mL),[44] glycan-based lateral flow detection system (5 μg/mL),[45] photoelectrochemical aptasensor (72 ng/mL),[46] nanobody-based ELISA (0.147 ng/mL),[47] and portable amperometric immunosensor (0.15 ng/mL).[48] Apparently, the method we developed exhibits a similar LOD as the OFET[42] but outperforms most methods in sensitivity for the detection of spike antigens. The good sensitivity contributes to the screened phage #2 expressing the NFWISPKLAFAL peptide from the display library of the pIII phage, which has an excellent affinity to SARS-CoV-2 S1. The second reason may be attributed to the M13 filamentous phage, which has approximately 2700 copies of the major pVIII capsid proteins for significant signal amplification when using a reporter-coupled secondary antibody (anti-M13-HRP mAb) specific for the pVIII proteins. Many studies have revealed that phages are greater reporter elements in immunoassays.[49]

Phage ELCLIA for Detection of SARS-CoV-2 Pseudoviruses. The spike protein of coronaviruses, particularly their RBD, is known to mutate frequently.[50] We tested phage #2 for binding to a pseudovirus SARS-CoV-2 (D614G). The pseudovirus was engineered to display the full trimeric S protein of SARS-CoV-2 within the viral envelope.[34,51] The surface of this pseudovirus resembles that of SARS-CoV-2, which can enter human cells but cannot replicate itself, allowing for its use in biosafety-level-2 labs as a model virus.[52] Considering that the exposure to SARS-CoV-2 or clinical samples from patients containing SARS-CoV-2 poses a high risk of infection, the virus was inactivated by heating at 65 °C for 30 min. As low as 30 transducing units (TU)/mL of inactivated pseudoviruses could be detected in PBS buffer (Figure 6A). Although saliva contains complex components that affect detection sensitivity, we could still detect as low as 60 TU/mL of inactivated pseudoviruses in 50% saliva (Figure 6B). Clinical samples are heat-inactivated to avoid infection during analysis, suggesting that our assay has better operational safety.

CONCLUSIONS

In summary, after four rounds of biopanning from the pIII phage display library, a phage monoclone expressing the NFWISPKLAFAL peptide was identified, which had the best affinity and selectivity for SARS-CoV-2 S1 with a dissociation constant of 3.45 ± 0.58 nM. Additionally, the screened peptide binds at the NTD of the S1 subunit through a hydrogen bond network and hydrophobic interaction, supported by molecular docking. Subsequently, a phage-based ELCLIA was established by using the obtained phage as a bifunctional probe with SARS-CoV-2 S1 antigen recognition and significant signal amplification. The proposed method exhibits good sensitivity with a LOD of 78 pg/mL SARS-CoV-2 S1 antigen. Furthermore, low to 60 TU/mL inactivated pseudoviruses in 50% saliva can be detected. Unfortunately, there are strict biological safety restrictions on the SARS-CoV-2-related experiment which was allowed to be performed only in authorized institutes or hospitals, and our lab does not have the qualification certificate to obtain real SARS-CoV-2 virus or clinical positive samples. In the future, the accuracy of phage-based ELCLIA will be verified by testing clinical samples from COVID-19 patients. Considering that phage monoclones can be obtained by simple culture and purification, similar ideas can be expanded to develop other biosensors with great potential for screening or diagnosing other biomarkers or possible future infectious-disease pandemics.

ASSOCIATED CONTENT

Supporting Information

The Supporting Information is available free of charge at https://pubs.acs.org/doi/10.1021/acs.analchem.2c01988.

Cartoon illustrating M13 phage, schematic illustration of the process to biopan the SARS-CoV-2 S1-binding phage, phage ELCLIA to detect SARS-CoV-2 S1, amino acid sequences for the displayed peptides of the selected phage clones, and summary of analytical performance for different methods to detect SARS-CoV-2 S1 (PDF)

AUTHOR INFORMATION

Corresponding Author

Aihua Liu − *Institute for Chemical Biology & Biosensing, College of Life Sciences, Qingdao University, Qingdao 266071, China;* orcid.org/0000-0003-4260-1982; Email: liuah@qdu.edu.cn

Authors

Junchong Liu − *Institute for Chemical Biology & Biosensing, College of Life Sciences, Qingdao University, Qingdao 266071, China*

Pengxin Ma − *Institute for Chemical Biology & Biosensing, College of Life Sciences, Qingdao University, Qingdao 266071, China*

Haipeng Yu − *Institute for Chemical Biology & Biosensing, College of Life Sciences, Qingdao University, Qingdao 266071, China*

Mingyang Wang − *Institute for Chemical Biology & Biosensing, College of Life Sciences, Qingdao University, Qingdao 266071, China*

Pengxue Yin − *Institute for Chemical Biology & Biosensing, College of Life Sciences, Qingdao University, Qingdao 266071, China*

Shuang Pang − *Institute for Chemical Biology & Biosensing, College of Life Sciences, Qingdao University, Qingdao 266071, China*

Yiming Jiao − *Institute for Chemical Biology & Biosensing, College of Life Sciences, Qingdao University, Qingdao 266071, China*

Tao Dong − *Institute for Chemical Biology & Biosensing, College of Life Sciences, Qingdao University, Qingdao 266071, China*

Complete contact information is available at:

https://pubs.acs.org/10.1021/acs.analchem.2c01988

Author Contributions

†J.L. and P.M. contributed equally to this work.

Notes

The authors declare no competing financial interest.

■ ACKNOWLEDGMENTS

This work was financially supported partially by the National Key Research and Development Program of China (2021YFA0910400) and National Natural Science Foundation of China (22174081 and 81673172).

■ REFERENCES

(1) Han, P.; Li, L.; Liu, S.; Wang, Q.; Zhang, D.; Xu, Z.; Han, P.; Li, X.; Peng, Q.; Su, C.; Huang, B.; Li, D.; Zhang, R.; Tian, M.; Fu, L.; Gao, Y.; Zhao, X.; Liu, K.; Qi, J.; Gao, G. F.; Wang, P. *Cell* **2022**, *185*, 630−640.

(2) Yin, W.; Xu, Y.; Xu, P.; Cao, X.; Wu, C.; Gu, C.; He, X.; Wang, X.; Huang, S.; Yuan, Q.; Wu, K.; Hu, W.; Huang, Z.; Liu, J.; Wang, Z.; Jia, F.; Xia, K.; Liu, P.; Wang, X.; Song, B.; Zheng, J.; Jiang, H.; Cheng, X.; Jiang, Y.; Deng, S.-J.; Xu, H. E. *Science* **2022**, *375*, 1048−1053.

(3) Nguyen, N. H. L.; Kim, S.; Lindemann, G.; Berry, V. *ACS Nano* **2021**, *15*, 11743−11752.

(4) Xia, B. Q.; Shen, X. R.; He, Y.; Pan, X. Y.; Liu, F. L.; Wang, Y.; Yang, F. P.; Fang, S.; Wu, Y.; Duan, Z. L.; Zuo, X. L.; Xie, Z. Q.; Jiang, X. R.; Xu, L.; Chi, H.; Li, S. Q.; Meng, Q.; Zhou, H.; Zhou, Y. B.; Cheng, X.; Xin, X. M.; Jin, L.; Zhang, H. L.; Yu, D. D.; Li, M. H.; Feng, X. L.; Chen, J. K.; Jiang, H. L.; Xiao, G. F.; Zheng, Y. T.; Zhang, L. K.; Shen, J. S.; Li, J.; Gao, Z. B. *Cell Res.* **2021**, *31*, 847−860.

(5) Yan, W.; Zheng, Y.; Zeng, X.; He, B.; Cheng, W. *Signal Transduct. Targeted Ther.* **2022**, *7*, 26.

(6) Escalera, A.; Gonzalez-Reiche, A. S.; Aslam, S.; Mena, I.; Laporte, M.; Pearl, R. L.; Fossati, A.; Rathnasinghe, R.; Alshammary, H.; van de Guchte, A.; Farrugia, K.; Qin, Y.; Bouhaddou, M.; Kehrer, T.; Zuliani-Alvarez, L.; Meekins, D. A.; Balaraman, V.; McDowell, C.; Richt, J. A.; Bajic, G.; Sordillo, E. M.; Dejosez, M.; Zwaka, T. P.; Krogan, N. J.; Simon, V.; Albrecht, R. A.; van Bakel, H.; García-Sastre, A.; Aydillo, T. *Cell Host Microbe* **2022**, *30*, 373−387.

(7) Cai, X.; Chen, M.; Prominski, A.; Lin, Y.; Ankenbruck, N.; Rosenberg, J.; Nguyen, M.; Shi, J.; Tomatsidou, A.; Randall, G.; Missiakas, D.; Fung, J.; Chang, E. B.; Penaloza-MacMaster, P.; Tian, B.; Huang, J. *Adv. Sci.* **2022**, *9*, 2103240.

(8) Zhang, Z.; Pandey, R.; Li, J.; Gu, J.; White, D.; Stacey, H. D.; Ang, J. C.; Steinberg, C.-J.; Capretta, A.; Filipe, C. D. M.; Mossman, K.; Balion, C.; Miller, M. S.; Salena, B. J.; Yamamura, D.; Soleymani, L.; Brennan, J. D.; Li, Y. *Angew. Chem.* **2021**, *60*, 24266−24274.

(9) Li, N.; Wang, X.; Tibbs, J.; Che, C.; Peinetti, A. S.; Zhao, B.; Liu, L.; Barya, P.; Cooper, L.; Rong, L.; Wang, X.; Lu, Y.; Cunningham, B. T. *J. Am. Chem. Soc.* **2022**, *144*, 1498−1502.

(10) Peeling, R. W.; Heymann, D. L.; Teo, Y.-Y.; Garcia, P. J. *Lancet* **2022**, *399*, 757−768.

(11) Dzuvor, C. K. O.; Tettey, E. L.; Danquah, M. K. *Wiley Interdiscip. Rev.: Nanomed. Nanobiotechnol.* **2022**, *14*, No. e1785.

(12) Dai, C.; Guo, M.; Wu, Y.; Cao, B.-P.; Wang, X.; Wu, Y.; Kang, H.; Kong, D.; Zhu, Z.; Ying, T.; Liu, Y.; Wei, D. *J. Am. Chem. Soc.* **2021**, *143*, 19794−19801.

(13) Kacherovsky, N.; Yang, L. F.; Dang, H. V.; Cheng, E. L.; Cardle, I. I.; Walls, A. C.; McCallum, M.; Sellers, D. L.; DiMaio, F.; Salipante, S. J.; Corti, D.; Veesler, D.; Pun, S. H. *Angew. Chem., Int. Ed.* **2021**, *60*, 21211−21215.

(14) McKay, S. L.; Tobolowsky, F. A.; Moritz, E. D.; Hatfield, K. M.; Bhatnagar, A.; LaVoie, S. P.; Jackson, D. A.; Lecy, K. D.; Bryant-Genevier, J.; Campbell, D.; Freeman, B.; Gilbert, S. E.; Folster, J. M.; Medrzycki, M.; Shewmaker, P. L.; Bankamp, B.; Radford, K. W.; Anderson, R.; Bowen, M. D.; Negley, J.; Reddy, S. C.; Jernigan, J. A.; Brown, A. C.; McDonald, L. C.; Kutty, P. K.; Prevention, C. D. C. I.; Control, T.; the, C. D. C. C.-S. L. G. *Ann. Intern. Med.* **2021**, *174*, 945−951.

(15) Lu, S.; Tong, X.; Han, Y.; Zhang, K.; Zhang, Y.; Chen, Q.; Duan, J.; Lei, X.; Huang, M.; Qiu, Y.; Zhang, D.-Y.; Zhou, X.; Zhang, Y.; Yin, H. *Nat. Biomed. Eng.* **2022**, *6*, 286−297.

(16) Peinetti, A. S.; Lake, R. J.; Cong, W.; Cooper, L.; Wu, Y.; Ma, Y.; Pawel, G. T.; Toimil-Molares, M. E.; Trautmann, C.; Rong, L.; Mariñas, B.; Azzaroni, O.; Lu, Y. *Sci. Adv.* **2021**, *7*, No. eabh2848.

(17) Tuna, M.; Woolfson, D. *Phage Display In Biotechnology and Drug Discovery*; Sidhu, S. S., Geyer, C. R., Eds.; CRC Press: Boca Raton, 2015; pp 275−285.

(18) Sidhu, S. S.; Geyer, C. R. *Phage Display in Biotechnology and Drug Discovery*, 2nd ed.; CRC Press: Boca Raton, 2005.

(19) Olofsson, L.; Ankarloo, J.; Andersson, P. O.; Nicholls, I. A. *Chem. Biol.* **2001**, *8*, 661−671.

(20) Smith, G. P.; Petrenko, V. A. *Chem. Rev.* **1997**, *97*, 391−410.

(21) Smith, G. P. *Science* **1985**, *228*, 1315−1317.

(22) Liu, P.; Han, L.; Wang, F.; Li, X.; Petrenko, V. A.; Liu, A. *Nanoscale* **2018**, *10*, 2825−2833.

(23) Qi, H.; Wang, F.; Petrenko, V. A.; Liu, A. *Anal. Chem.* **2014**, *86*, 5844−5850.

(24) Lang, Q.; Wang, F.; Yin, L.; Liu, M.; Petrenko, V. A.; Liu, A. *Anal. Chem.* **2014**, *86*, 2767−2774.

(25) Han, L.; Liu, P.; Zhang, H.; Li, F.; Liu, A. *Chem. Commun.* **2017**, *53*, 5216−5219.

(26) Liu, P.; Han, L.; Wang, F.; Petrenko, V. A.; Liu, A. *Biosens. Bioelectron.* **2016**, *82*, 195−203.

(27) Yin, L.; Luo, Y.; Liang, B.; Wang, F.; Du, M.; Petrenko, V. A.; Qiu, H.-J.; Liu, A. *Antiviral Res.* **2014**, *109*, 68−71.

(28) Wang, G.; Yin, P.; Wang, J.; Ma, P.; Wang, Y.; Cai, Y.; Qi, H.; Liu, A. *Sens. Actuators, B* **2021**, *333*, 129555.

(29) Han, L.; Xia, H.; Yin, L.; Petrenko, V. A.; Liu, A. *Biosens. Bioelectron.* **2018**, *106*, 1−6.

(30) Wang, Y.; Wang, M.; Yu, H.; Wang, G.; Ma, P.; Pang, S.; Jiao, Y.; Liu, A. *Sens. Actuators, B* **2022**, *367*, 132009.

(31) Sasso, E.; D'Avino, C.; Passariello, M.; D'Alise, A. M.; Siciliano, D.; Esposito, M. L.; Froechlich, G.; Cortese, R.; Scarselli, E.; Zambrano, N.; Nicosia, A.; De Lorenzo, C. *mAbs* **2018**, *10*, 1060−1072.

(32) Wrapp, D.; Wang, N.; Corbett, K. S.; Goldsmith, J. A.; Hsieh, C. L.; Abiona, O.; Graham, B. S.; McLellan, J. S. *Science* **2020**, *367*, 1260−1263.

(33) Rahman, N.; Basharat, Z.; Yousuf, M.; Castaldo, G.; Rastrelli, L.; Khan, H. *Molecules* **2020**, *25*, 2271.

(34) Ou, X.; Liu, Y.; Lei, X.; Li, P.; Mi, D.; Ren, L.; Guo, L.; Guo, R.; Chen, T.; Hu, J.; Xiang, Z.; Mu, Z.; Chen, X.; Chen, J.; Hu, K.; Jin, Q.; Wang, J.; Qian, Z. *Nat. Commun.* **2020**, *11*, 1620.

(35) Yu, Z.; Kan, R.; Ji, H.; Wu, S.; Zhao, W.; Shuian, D.; Liu, J.; Li, J. *Food Chem.* **2021**, *342*, 128366.

(36) Wang, F.; Yang, Y.-Y.; Wan, D.-B.; Li, J.-D.; Liang, Y.-F.; Li, Z.-F.; Shen, Y.-D.; Xu, Z.-L.; Yang, J.-Y.; Wang, H.; Gettemans, J.; Hammock, B. D.; Sun, Y.-M. *Food Control* **2022**, *136*, 108835.

(37) Cinquanta, L.; Fontana, D. E.; Bizzaro, N. *Autoimmun. Highlights* **2017**, *8*, 9.

(38) Kim, J. S.; Taitt, C. R.; Ligler, F. S.; Anderson, G. P. *Sens. Instrum. Food Qua. Saf.* **2010**, *4*, 73−81.

(39) Lewis, T.; Giroux, E.; Jovic, M.; Martic-Milne, S. *Analyst* **2021**, *146*, 7207−7217.

(40) Lee, J. H.; Choi, M.; Jung, Y.; Lee, S. K.; Lee, C. S.; Kim, J.; Kim, J.; Kim, N. H.; Kim, B. T.; Kim, H. G. *Biosens. Bioelectron.* **2021**, *171*, 112715.

(41) Liu, D.; Ju, C. H.; Han, C.; Shi, R.; Chen, X. H.; Duan, D. M.; Yan, J. H.; Yan, X. Y. *Biosens. Bioelectron.* **2021**, *173*, 112817.

(42) Ditte, K.; Nguyen Le, T. A.; Ditzer, O.; Sandoval Bojorquez, D. I.; Chae, S.; Bachmann, M.; Baraban, L.; Lissel, F. *ACS Biomater. Sci. Eng.* **2021**, DOI: 10.1021/acsbiomaterials.1c00727.

(43) Agarwal, D. K.; Nandwana, V.; Henrich, S. E.; Josyula, V.; Thaxton, C. S.; Qi, C.; Simons, L. M.; Hultquist, J. F.; Ozer, E. A.;

Shekhawat, G. S.; Dravid, V. P. *Biosens. Bioelectron.* **2022**, *195*, 113647.
(44) Fabiani, L.; Saroglia, M.; Galatà, G.; De Santis, R.; Fillo, S.; Luca, V.; Faggioni, G.; D'Amore, N.; Regalbuto, E.; Salvatori, P.; Terova, G.; Moscone, D.; Lista, F.; Arduini, F. *Biosens. Bioelectron.* **2021**, *171*, 112686.
(45) Baker, A. N.; Richards, S.-J.; Guy, C. S.; Congdon, T. R.; Hasan, M.; Zwetsloot, A. J.; Gallo, A.; Lewandowski, J. R.; Stansfeld, P. J.; Straube, A.; Walker, M.; Chessa, S.; Pergolizzi, G.; Dedola, S.; Field, R. A.; Gibson, M. I. *ACS Cent. Sci.* **2020**, *6*, 2046−2052.
(46) Jiang, Z. W.; Zhao, T. T.; Li, C. M.; Li, Y. F.; Huang, C. Z. *ACS Appl. Mater. Interfaces* **2021**, *13*, 49754−49761.
(47) Girt, G. C.; Lakshminarayanan, A.; Huo, J. D.; Dormon, J.; Norman, C.; Afrough, B.; Harding, A.; James, W.; Owens, R. J.; Naismith, J. H. *R. Soc. Open Sci.* **2021**, *8*, 211016.
(48) Erdem, A.; Senturk, H.; Yildiz, E.; Maral, M. *Talanta* **2022**, *244*, 123422.
(49) Mao, C.; Liu, A.; Cao, B. *Angew. Chem.* **2009**, *48*, 6790−6810.
(50) Starr, T. N.; Greaney, A. J.; Hilton, S. K.; Ellis, D.; Crawford, K. H. D.; Dingens, A. S.; Navarro, M. J.; Bowen, J. E.; Tortorici, M. A.; Walls, A. C.; King, N. P.; Veesler, D.; Bloom, J. D. *Cell* **2020**, *182*, 1295−1310.
(51) Crawford, K. H. D.; Eguia, R.; Dingens, A. S.; Loes, A. N.; Malone, K. D.; Wolf, C. R.; Chu, H. Y.; Tortorici, M. A.; Veesler, D.; Murphy, M.; Pettie, D.; King, N. P.; Balazs, A. B.; Bloom, J. D. *Viruses* **2020**, *12*, 513.
(52) Chen, X. Y.; Li, R.; Pan, Z. W.; Qian, C. F.; Yang, Y.; You, R. R.; Zhao, J.; Liu, P. H.; Gao, L. Q.; Li, Z. R.; Huang, Q. H.; Xu, L. F.; Tang, J. F.; Tian, Q.; Yao, W.; Hu, L.; Yan, X. F.; Zhou, X. Y.; Wu, Y. H.; Deng, K.; Zhang, Z.; Qian, Z. H.; Chen, Y. K.; Ye, L. L. *Cell. Mol. Immunol.* **2020**, *17*, 647−649.

https://doi.org/10.1021/acs.analchem.2c01988
Anal. Chem. 2022, 94, 11591−11599